Pattern Formation in Two-Dimensional Turbulence on a Rotating Sphere

Shigeo Yoden[1], Keiichi Ishioka[2], Michio Yamada[2], and Yoshi-Yuki Hayashi[3]

[1] Department of Geophysics, Kyoto University, Kyoto, 606-8502, Japan
[2] Graduate School of Mathematical Sciences, University of Tokyo, Tokyo, 153-8914, Japan
[3] Division of Earth and Planetary Sciences, Hokkaido University, Sapporo 060-0810, Japan

Abstract. Series of numerical experiments on two-dimensional decaying turbulence are performed for a non-divergent barotropic fluid on a rotating sphere to survey the nature of pattern formation from random initial fields. Time evolution of the flow field is highly dependent on the rotation rate of the system. In non-rotational cases, isolated coherent vortices emerge in the course of time development as in the planar two-dimensional turbulence. As the rotation rate increases, however, the evolution of the flow field changes drastically, and a westward circumpolar vortex appears in high-latitudes as well as zonal band structures in mid- and low-latitudes. Dependence of these features on the initial energy spectrum is investigated and the dynamics of such pattern formations is discussed with a weakly nonlinear Rossby wave-zonal flow interaction theory.

1 Introduction

An interesting feature of two-dimensional turbulence is the emergence of isolated coherent vortices found by McWilliams [1,2], which is due to a self-organizing mechanism involved in the disorder two-dimensional motion. As an application to geophysical fluid, Rhines [3] firstly studied the two-dimensional turbulence on a β-plane [4] to understand the effect of differential rotation of planet. His numerical result showed the anisotropic growth of flow field and the emergence of alternating bands of mean zonal current. These features of the β effect have been reconfirmed in recent numerical studies with much higher resolution models [5,6]. Williams [7] took account of the exact spherical geometry in his numerical experiment on forced two-dimensional turbulence, aiming at a reproduction of the zonal band structure of Jovian atmosphere due to the β-effect. He obtained a clear band structure of zonal flow for a stochastic vorticity forcing. However, both longitudinal periodicity and equatorial symmetry were assumed in his experiment to reduce the computational domain to 1/16 of the entire sphere.

Advancement of computing facilities in 1990's enabled us to do these computations with higher resolutions in full spherical geometry [8–13]. In the decaying turbulence experiments [8], the emergence of a westward circumpolar vortex was found in high-latitudes for high-rotation cases, in addition to the spontaneous formation of the zonal band structures in mid- and low-latitudes. Such

formation of a circumpolar vortex was also observed in the forced turbulence experiment [10] and a laboratory experiment with rotating tank [14].

In this article, recent studies on the two-dimensional decaying turbulence on a rotating sphere by ourselves [15,16] are summarized with emphasis on the pattern formation due to full nonlinear upward cascade of turbulent energy in small scales and the role of Rossby waves in angular momentum redistribution. Possible application to some phenomena in real geophysical fluids is also discussed.

2 Numerical Model and Experiments

Freely-evolving two-dimensional non-divergent flow on a rotating sphere is governed by the following vorticity equation:

$$\frac{\partial \omega}{\partial t} + \frac{1}{a^2} J(\psi, \omega) + \frac{2\Omega}{a^2} \frac{\partial \psi}{\partial \lambda} = (-1)^{p+1} \nu_{2p} \left(\Delta + \frac{2}{a^2} \right)^p \omega, \tag{1}$$

where $\psi(\lambda, \mu, t)$ is a streamfunction field, $\omega(\lambda, \mu, t)$ the vertical component of vorticity ($\equiv \Delta\psi$), λ the longitude, $\mu \equiv \sin\phi$ with the latitude ϕ, t the time, $J(A, B)$ the horizontal Jacobian, Δ the horizontal Laplacian, a the radius of the sphere, Ω the rotation rate of the sphere. On the right hand side hyper-viscosity of the order of p is assumed with a viscosity coefficient ν_{2p}. In the case of $\nu_{2p} = 0$, (1) means the conservation of potential vorticity (hereafter denoted as PV; in the present case it is equivalent to absolute vorticity) $q \equiv \omega + 2\Omega\mu$ following Lagrangian motion.

To construct a spectral model of (1), we expand a dependent variable $\psi(\lambda, \mu, t)$ into a set of spherical harmonics,

$$\psi(\lambda, \mu, t) = \sum_{n=2}^{N} \sum_{m=-n}^{n} \psi_n^m(t) P_n^m(\mu) e^{im\lambda}, \tag{2}$$

and truncate it at the total wavenumber $N = 341$ (i.e., triangular truncation T341). A spectral transform method [17] is used to compute the nonlinear Jacobian term; grids for the spectral transformation is 1024(longitude)×512(latitude).

Time evolution of $\psi(\lambda, \mu, t)$ is computed from an initial random flow field, of which energy spectrum is given by

$$E(n, t=0) = \frac{An^5}{e^{-n/2}}, \qquad \text{or,} \qquad E(n, t=0) = \frac{An^{\gamma/2}}{(n+n_0)^\gamma}. \tag{3}$$

Here the energy density is given by $E(n,t) = \frac{1}{2} n(n+1) \sum_{m=-n}^{n} |\psi_n^m(t)|^2$. Each complex amplitude $\psi_n^m(t=0) = (-1)^m (\psi_n^{-m}(t=0))^*$ (where * denotes complex conjugate) is determined so that it has random amplitude and random phase under the above constraint. The former expression in (3) was assumed in [8] while the latter was used in [9]. A constant A is set so that the total kinetic energy is unity without dimension: $\mathcal{E}(t=0) = \sum_{n=2}^{N} E(n, t=0) = 1$.

Table 1. Description of the initial parameters for each experimental set and decay rates of total energy, $\mathcal{E}(t=5)/\mathcal{E}(t=0)$, and enstrophy, $\mathcal{Q}(t=5)/\mathcal{Q}(t=0)$. These ratios depending on the rotation rate Ω are listed in %, which are ensemble averages of 10 runs from the initial conditions made with different random numbers

set name	yy1993 [8]		cpn010		cpn050 <control>		cpn100		cpg100	
n_0	—		10		50		100		50	
γ	—		1000		1000		1000		100	
$\mathcal{Q}(t=0)$	180.0		111.7		2590.7		10262.1		2992.0	
Ω	$\mathcal{E}$[%]	$\mathcal{Q}$[%]	$\mathcal{E}$[%]	$\mathcal{Q}$[%]	$\mathcal{E}$[%]	$\mathcal{Q}$[%]	$\mathcal{E}$[%]	$\mathcal{Q}$[%]	$\mathcal{E}$[%]	$\mathcal{Q}$[%]
0	99.8	25.9	99.9	35.4	97.5	10.3	89.7	5.3	97.1	10.5
25	99.8	24.8	99.9	40.6	97.4	7.6	89.6	4.3	97.0	7.8
50	99.8	29.9	99.9	51.3	97.3	5.5	89.5	3.1	96.9	5.6
100	99.9	40.8	100.0	67.9	97.3	4.2	89.3	1.8	96.9	4.0
200	99.9	53.3	100.0	78.4	97.3	5.1	89.3	1.4	96.9	4.6
400	99.9	65.3	100.0	87.7	97.4	7.6	89.3	1.9	96.9	6.5

Computations are done in a non-dimensional form. The radius of the sphere is taken as a length scale (L); $a = 1$ in the non-dimensional form. Advective time scale is adopted; the time scale (T) is equal to the length scale divided by square root of mean kinetic energy (or velocity scale U). If we take a rough scaling for the atmosphere as $U \sim 10$ m/s and $L = 6 \times 10^6$ m, the time scale is $T \sim L/U = 6 \times 10^5$ s ~ 7 days. Six values of Ω are taken as an experimental parameter: 0, 25, 50, 100, 200 and 400. The sphere has $\Omega/(2\pi)$ rotations per unit time interval. If we take the above scaling, $\Omega = 50$ is close to the present rotation of the earth.

The parameter values of the initial energy spectrum used in the present study are listed in Table 1 and the spectra are shown in Fig.1. Five vertical dash-lines in the figure indicate a characteristic wavenumber $n_\beta \equiv \{\pi\Omega/(4U)\}^{1/2} = \{\pi\Omega/(4\sqrt{2\mathcal{E}})\}^{1/2}$ for each Ω; at the spatial scale with n_β, the linear rotation term is comparable to the nonlinear Jacobian term in (1). Note that the initial energy spectrum used in [8], denoted by a solid line, has much energy in large scales of $n < n_\beta|_{\Omega=400}$; even in the highest rotation case of $\Omega = 400$ the linear term dominates from the initial time. On the other hand, the spectral form used in [9], the latter in (3), can limit the initial energy distribution near n_0 for a large value of γ. Here we use five sets of initial conditions including the reexamination of [8] with higher resolution(denoted as yy1993); the control experiment(cpn050) is given by $(n_0, \gamma) = (50, 1000)$. The spectral peak of initial energy is located in much larger wavenumber than n_β in the three experimental sets with $n_0 = 50$ or 100(cpn050, cpn100 and cpg100).

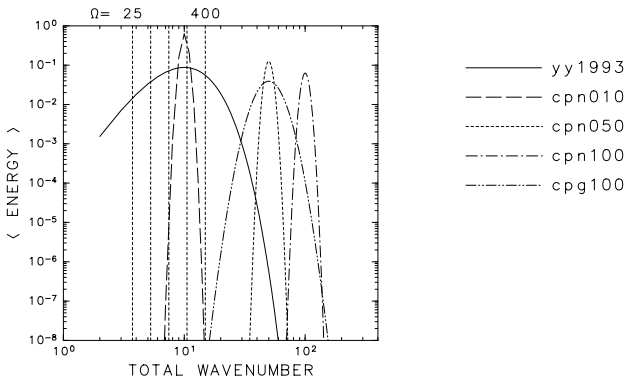

Fig. 1. Five initial energy spectra given by (3) with parameter values listed in Table 1. Vertical dash-lines indicate the characteristic wavenumber $n_\beta = \{\pi\Omega/(4\sqrt{2})\}^{1/2}$ for five values of Ω; 25, 50, 100, 200 and 400

The hyper-viscosity is set with $p = 8$ and $\nu_{2p} = 1 \times 10^{-38}$. Ten initial conditions are made with different random numbers for each experimental set, and time evolutions from these are computed until $t = 5$ by the fourth-order Runge-Kutta method with the time increment of $\Delta t = 1 \times 10^{-3}$. All of the computations are done in double precision.

3 Results

Time variations of the total energy and the total enstrophy are not very sensitive to the value of Ω. The total energy dissipates about 2% by $t = 1$ and it is nearly conservative afterward in the control run [15]. On the other hand, the total enstrophy has a maximum dissipation rate around $t \sim 0.2$ and decays as $\mathcal{Q}(t) \propto t^{-1}$ after that time. Decay rates of the total energy and the total enstrophy for the integration period are also listed in Table 1 for the five experimental sets. The energy is almost conserved for the cases in which the spectral peak of the initial energy is located in a low wavenumber (yy1993 and cpn010), while the energy decay is about 10 % when the spectral peak is at $n = 100$ (cpn100). On the other hand, the enstrophy decay is dependent on the initial energy spectra. The decay rate is smaller if the spectral peak is at a lower wavenumber, particularly for the cases of large Ω.

Time evolution of the energy spectrum $E(n,t)$ is dependent on the initial spectrum and the rotation rate as reported in [15]. For the high-rotation case of $\Omega = 400$, however, a power law close to n^{-4} is obtained for all cases in a wide range, extending to low wavenumbers less than n_β.

Time evolution of the flow field can be viewed by movies of the PV and the vorticity fields [18]. Figure 2 shows some snapshots of the vorticity field for a non-rotational case in the control experiment. The initial vorticity field is homo-

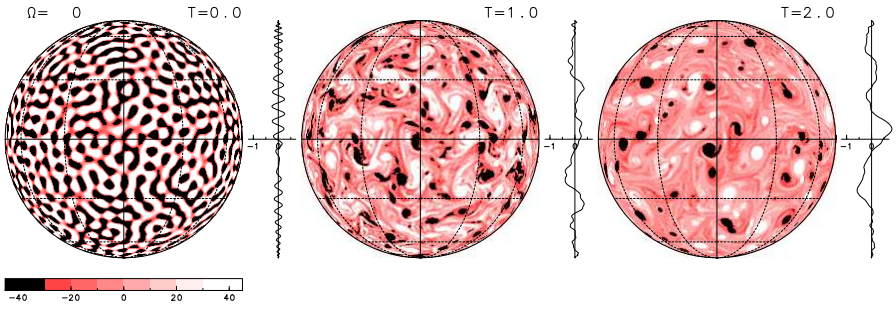

Fig. 2. Time evolution of the vorticity field for $\Omega = 0$ in the control experiment: (left) $t = 0$, (center) $t = 1$, and (right) $t = 2$. Orthographic projection from $\lambda = 0^\circ$, $\phi = 0^\circ$ is used and lines of meridians and parallels are drawn for every 30°. Solid line on the right side of each panel shows the zonal mean zonal angular momentum as a function of sine latitude

geneous and isotropic due to random initial condition. At $t = 1$, high-gradient, filamentary structures are created, which are indicative of the dissipation of enstrophy in small scales, and eventually isolated coherent vortices emerge as in the planar two-dimensional turbulence [1,2] through mergers of vortices with the same sign of vorticity.

The time evolution is largely dependent on the rotation rate Ω. Figure 3 is an example to show the dependence of vorticity field at $t = 5$ evolved from the same initial condition shown in Fig.2(left) on the rotation rate. In the non-rotational case (left), number of the coherent vortices decreases from $t = 2$ shown in Fig.2(right) owing to their mergers, and filamentary structures dim out after large enstrophy dissipation. In the high-rotation case of $\Omega = 400$(right), on the other hand, the vorticity field is not isotropic but shows zonally elongated structures. The zonal mean zonal angular momentum shows the emergence of westward circumpolar vortex, particularly in the southern hemisphere for this run, as well as zonal band structures in mid- and low-latitudes. Movies of the PV field for rotational cases clearly show westward propagation of the disturbance as Rossby waves generated through the upward energy cascade [18]. Note that the energy spectrum with n^{-4} power law should be related to the vorticity distribution with sharp contrast shown in Fig.3(right).

Figure 4 shows time evolutions of the zonal mean zonal angular momentum for six values of Ω starting from the same initial condition in the control experiment. The formation of westward circumpolar vortex in high latitudes and zonal band structure of alternating mean zonal jets in mid- and low-latitudes can be clearly seen as the increase of Ω. The band structure develops from an early stage of the time evolution. At the beginning of integration, the mean zonal angular momentum profile has a rather high characteristic latitudinal wavenumber, and the characteristic wavenumber evolves rapidly toward lower value. Around $t \sim 0.5$, the band structure comes to a steady or very slowly evolving state,

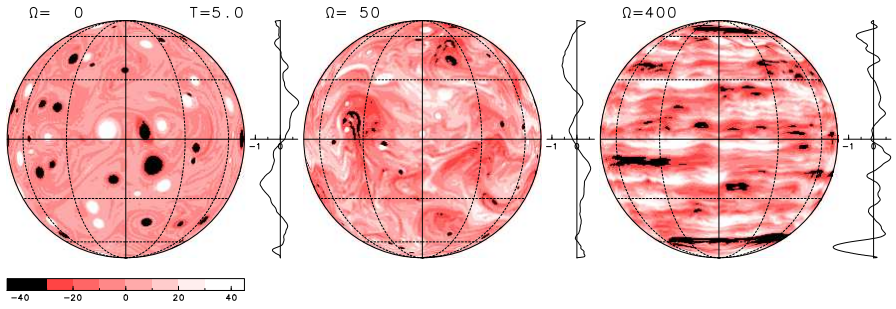

Fig. 3. Vorticity field at $t = 5$ depending on the rotation rate in the control experiment: (left) $\Omega = 0$, (center) $\Omega = 50$, and (right) $\Omega = 400$. The same projection as in Fig.2 is used. The zonal mean zonal angular momentum is also shown

and their latitudinal positions are hardly changed with time afterwards. Generally the number of the jets increases while the width of them decreases, as the rotation rate Ω increases. The characteristic wavenumber of the zonal band structure seems to be roughly proportional to n_β as shown in [10] for the forced two-dimensional turbulence on a rotating sphere. It should be noted that the latitudinal positions of mean zonal jets are crucially dependent on the initial condition made with 10 different random numbers.

Dependence of the zonal mean zonal angular momentum at $t = 5$ on Ω is shown in Fig.5 for the five experimental sets with different spectral profiles. The formation of westward circumpolar vortex for large Ω is a robust result independent of the choice of the initial energy spectrum. As Ω increases, the intensity of the westward vortex becomes large and its maximum position shifts toward higher latitudes. Note that the westward vortex for $\Omega = 400$ is stronger for the larger value of n_0 from the set cpn010 to cpn100. As a result of the ensemble average, eastward flow appears in mid- and low-latitudes for large Ω cases owing to the conservation of total angular momentum. However, each realization shows a zonal band structure in these latitudes. The ensemble average masks the band structure because the latitudinal positions of the jets depend rather randomly on each realization.

4 Discussion

It was confirmed that the westward circumpolar vortex is a robust feature of two-dimensional decaying turbulence on a rapidly rotating sphere. Hayashi et al. [16] investigated the dynamics of the formation of the circumpolar vortex with the framework of a weakly nonlinear Rossby wave-zonal flow interaction theory, and the essence is summarized here.

The important quantity that characterizes two dimensional non-divergent flow on a rotating sphere is the transition wavenumber defined as a local wavenumber at which the magnitude of the nonlinear Jacobian term in (1) is comparable

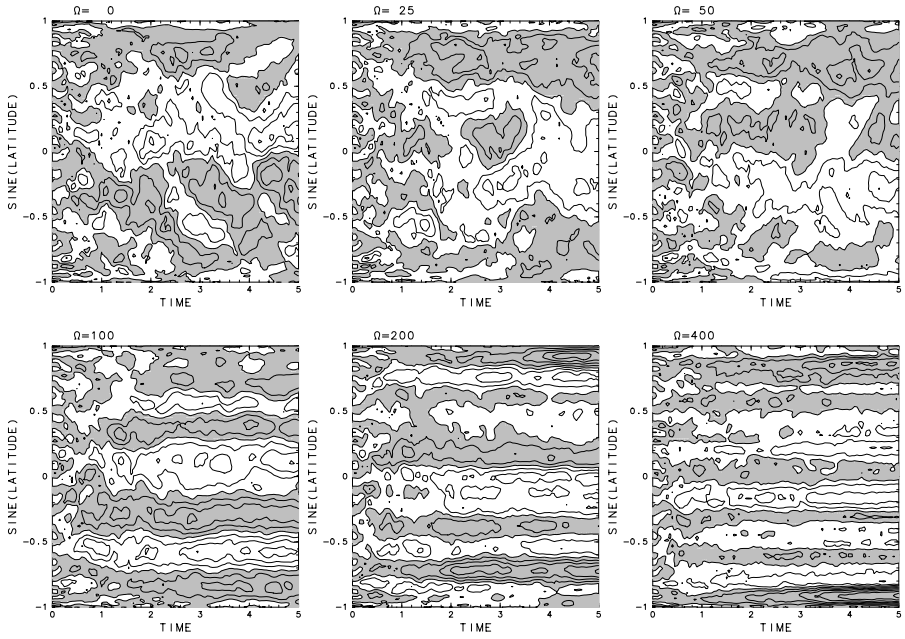

Fig. 4. Time evolutions of the zonal mean zonal angular momentum from the same initial condition of cpn050 for $\Omega = 0$, 25 and 50(top), while 100, 200 and 400(bottom). Contour interval is 0.25 and negative westward flow is shaded

to that of the linear advection term of the planetary vorticity(the third term in (1), so called β term) [3,6,19]. The transition wavenumber may be written as $k_\beta(\phi) = \sqrt{2\Omega \cos\phi}$. When a local characteristic wavenumber of the flow is larger than $k_\beta(\phi)$, the nonlinear term dominates and turbulent motion appears, while Rossby waves dominate when it is smaller than $k_\beta(\phi)$. On a rotating sphere the transition wavenumber vanishes at the poles, while it is maximum at the equator since the β effect is largest at the equator. This implies that, for a disturbance with a given characteristic scale, flow becomes turbulent more easily in the polar region than in the lower latitudes. Provided that the characteristic wavenumber of the flow is $\tilde{n}$, a Rossby-wave dominant region appears around the equator between latitudes $\phi_t = \pm\cos^{-1}[\tilde{n}^2/(2\Omega)]$ when the rotation is sufficiently large.

In all the runs for high rotation cases, the characteristic wavenumber $\tilde{n}$ is about 10 or less, and the transition latitude from wavy to turbulent regime becomes $\phi_t \geq \pm 83^\circ$ for $\Omega = 400$. The formation of the westward circumpolar vortex may be considered as a result of turbulent mixing of PV in the polar region where the flow regime is regarded as turbulent. On a rotating sphere, the homogenization of PV due to mixing of the higher PV around the pole and the lower one in the lower latitudes causes westward flow in the polar region [14,19],

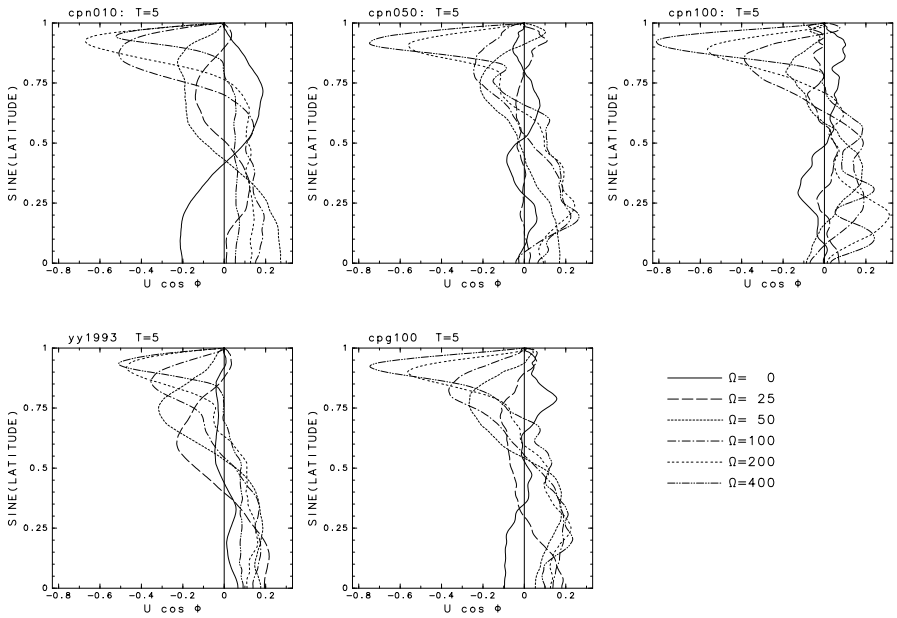

Fig. 5. Dependence of the zonal mean zonal angular momentum at $t = 5$ on the rotation rate Ω for the five initial energy spectra: (top) cpn010, cpn050 and cpn100, (bottom) yy1993 and cpg100. Ensemble average of 2×10 runs is shown under the assumption of equatorial symmetry

provided that there is no net positive angular momentum supply from the outside of the polar mixed region.

When the rotation rate is high and the outside of the polar mixed region is regarded as in the Rossby wave regime, it can be demonstrated that the net angular momentum supply from the outside of the polar mixed region is negative(westward). As is expected from the knowledge that the pseudo angular momentum associated with Rossby waves is negative, the key issue is whether the polar mixed region absorbs Rossby waves from the wavy region to gain westward momentum or radiates Rossby waves toward the wavy region to gain eastward momentum.

Weak nonlinear theory on the wave mean-flow interaction of Rossby waves on a sphere applied for the present experimental framework gives the result of westward momentum accumulation in high latitudes [16]. WKBJ theory of Rossby wave propagation on a rotating sphere [20,21] shows that a Rossby wave packet propagates along a great circle as seen from the frame of rotation with the speed of eastward phase velocity of the wave packet. A Rossby wave packet whose pitch angle at the equator is sufficiently large can propagate into the polar region where β is small. The propagation of such wave packets induces the second order

westward flow, particularly in higher latitudes due to the spherical effect, since the angular momentum associated with the wave packet is conserved during its propagation. If the wave mean-flow interaction takes place, we can expect that large westward fluctuation of mean zonal flow in the higher latitudes enhances the critical latitude absorption there, which contributes the westward momentum accumulation in the polar region.

The above weak nonlinear scenario was examined by a numerical comparison between the nonlinear and weakly nonlinear evolutions starting from the same initial condition [16]. The weakly nonlinear system gives very similar results as the full nonlinear ones for the cases of $\Omega = 400$; the accumulation of the westward angular momentum occurs in the polar region very similarly, and the eastward flow acceleration continues steadily. The resemblance between the nonlinear and weakly nonlinear evolutions is fairly good in the cases of $\Omega = 200$, while the evolution of the mean zonal flow is occasionally different in mid- and low-latitudes in the cases of $\Omega = 100$.

Pattern formation in two-dimensional turbulence on a rotating sphere may be applied for understanding some phenomena in real geophysical fluids. The formation of zonal band structure from a random flow field has been considered as a mechanism to explain the bands in the atmospheres on the giant outer planets such as Jupiter, Saturn, Uranus and Neptune [7,22]. Westward zonal flow in high latitudes in the sun [23] has superficial similarity to the circumpolar vortex obtained in the present study. Recently numerical study of the solar tachocline was also done by investigating freely evolving stratified turbulence in a thin rotating spherical shell [24].

Annular variability observed in both hemispheres of the atmosphere [25,26] is a modulation in the strength of the circumpolar vortex in the troposphere and lower stratosphere with intraseasonal and interannual time scales. Variations of the mean zonal jets with significant barotropic components have much connection with time variations of meridional and vertical PV flux [27], and key dynamics of the annular variability may be identical with that of the formation of the present circumpolar vortex [14].

5 Conclusions

Series of numerical experiments on the two-dimensional decaying turbulence on a rotating sphere were performed with a high-resolution spectral model. Pattern formation due to a self-organizing mechanism in turbulent motion is dependent on the rotation rate of the sphere. The main results are summarized as follows:

1. The flow field becomes anisotropic owing to the effect of rotation. A westward circumpolar vortex appears in high latitudes and zonal band structures of alternating mean zonal jets appear in mid- and low-latitudes for high-rotation cases.
2. The formation of the westward circumpolar vortex is a robust feature of the two-dimensional decaying turbulence on a rapidly rotating sphere and insensitive to the choice of the initial energy spectrum.

3. The zonal band structures are discernible from an early stage of the time evolution, and once established their latitudinal positions are hardly changed with time. As the rotation rate increases, the number of the jets increases while the width of them decreases.

References

1. J.C. McWilliams: J. Fluid Mech. **146**, 21 (1984)
2. J.C. McWilliams: J. Fluid Mech. **219**, 361 (1990)
3. P.B. Rhines: J. Fluid Mech. **69**, 417 (1975)
4. J. Pedlosky: *Geophysical Fluid Dynamics*, 2nd edn. (Springer, New York 1987)
5. M.E. Maltrud, G.K. Vallis: J. Fluid Mech. **228**, 321 (1991)
6. G.K. Vallis, M.E. Multrad: J. Phys. Oceanogr. **23**, 1346 (1993)
7. G.P. Williams: J. Atmos. Sci. **35**, 1399 (1978)
8. S. Yoden, M. Yamada: J. Atmos. Sci. **50**, 631 (1993)
9. J.Y-K. Cho, L.M. Polvani: Phys. Fluids **8**, 1531 (1996)
10. T. Nozawa, S. Yoden: Phys. Fluids **9**, 2081 (1997)
11. T. Nozawa, S. Yoden: Phys. Fluids **9**, 3834 (1997)
12. H.P. Huang, W.A. Robinson: J. Atmos. Sci. **55**, 611 (1998)
13. K. Ishioka, M. Yamada, Y.-Y. Hayashi, S. Yoden: Nonlinear Processes in Geophys. **7**, 105 (2000)
14. P.B. Rhines: 'Rossby Waves and the Polar Vortex'. In: *http://www.ocean.washington.edu/research/gfd/rossby.html* (1998)
15. S. Yoden, K. Ishioka, Y.-Y. Hayashi, M. Yamada: Il Nuovo Cimento C **22**, 803 (1999)
16. Y-Y. Hayashi, K. Ishioka, M. Yamada, S. Yoden: 'Emergence of circumpolar vortex in two dimensional turbulence on a rotating sphere'. In: *IUTAM Symposium on Developments in Geophysical Turbulence*. ed. by R.M. Kerr and Y. Kimura (Kluwer Academic Pub., Dordrecht, 2000) pp. 179–192.
17. W.M. Washington, C.L. Parkinson: *An introduction to three-dimensional climate modeling* (University Science Books, Mill Valley 1986)
18. K. Ishioka, M. Yamada, Y.-Y. Hayashi, S. Yoden: Nagare Multimedia(Nagare) **18**, (1999). Also in: *http://www.nagare.or.jp/mm/99/index.htm*
19. P.B. Rhines: Chaos **4**, 313 (1994)
20. B.J. Hoskins, D.J. Karoly: J. Atmos. Sci. **38**, 1179 (1981)
21. Y-Y. Hayashi, T. Matsuno: J. Met. Soc. Japan **62**, 377 (1984)
22. J.Y-K. Cho, L.M. Polvani: Science **273**, 335 (1996)
23. T.E. Dowling, E.A. Spiegel: *NonLinear Astrophysical Fluid Dynamics, Ann. NY Acad. Sci.* 190 (1990)
24. M.S. Miesch: Astrophys. J. **562**, 1058 (2001)
25. D.W.J. Thompson, J.M. Wallace: Geophys. Res. Lett. **25**, 1297 (1998)
26. D.W.J. Thompson, J.M. Wallace: J. Climate **13**, 1000 (2000)
27. D.L. Hartmann, J.M. Wallace, V. Limpasuvan, D.W.J. Thompson, J.R. Holton: Proc. Nat. Acad. Sci. **97**, 1412 (2000)